

## Highly ordered mesoporous zirconia-polyoxometalate nanocomposite materials for catalytic oxidation of alkenes

Gerasimos S. Armatas,<sup>\*a</sup> Georgios Bilis<sup>b</sup> and Maria Louloudi<sup>b</sup>

Received 8th October 2010, Accepted 29th November 2010

DOI: 10.1039/c0jm03395b

A series of well-ordered mesoporous ZrO<sub>2</sub>-based heteropoly acid nanocomposite frameworks has been prepared through a surfactant-assisted sol-gel copolymerization route. The pore walls of these materials consist of nanocrystalline tetragonal ZrO<sub>2</sub> and Keggin-type 12-phosphomolybdic acid (PMA) components with different PMA loadings, *i.e.* 12, 22 and 37 wt%. Small angle X-ray scattering, high-resolution TEM and N<sub>2</sub> physisorption measurements indicated mesoporous property in hexagonal *p6mm* symmetry with large internal BET surface areas and narrow-sized pores. The incorporated PMA clusters preserve intact their Keggin structure into the mesoporous frameworks according to EDX, FT-IR and diffuse-reflectance UV/vis/NIR spectroscopy. The obtained ZrO<sub>2</sub>-PMA nanocomposites demonstrated great application potential in oxidative catalysis, exhibiting exceptional stability and catalytic activity in oxidation of alkenes using hydrogen peroxide as oxidant.

## 1. Introduction

The development of nanocomposite catalysts with large internal surface area and well-ordered pore structure has been a challenge for a long time. The synthesis of these materials is demanding and requires precise control and manipulation of starting building blocks on the nanoscale range. These materials can blend different features into the inorganic structure such as regular mesoporosity and high catalytic activity, which are derived from starting components. For this reason, for example, the construction of novel catalytic and magnetic materials requires the use of appropriate building units that undergo fast and reversible redox transformation and controllable localization and delocalization of spin transitions.<sup>1</sup>

The metal-oxygen clusters of the early transition metals (V, Nb, Mo, Ta, W) in their highest oxidation states, also known as polyoxometalates (POMs), offer interesting and exciting perspectives for this direction. The plethora of structural and compositional types in these compounds makes them suitable for applications in catalysis, magnetism, non-linear optics and medicine.<sup>2</sup> Among polyoxometalates, the Keggin-type anions constituted by twelve corner and edge-sharing MO<sub>6</sub> octahedrals around a central XO<sub>4</sub><sup>3-/4-</sup> tetrahedron ( $\{X^{n+}M_{12}O_{40}\}^{(8-n)-}$ , where X = P<sup>5+</sup>, As<sup>5+</sup>, Si<sup>4+</sup>, Ge<sup>4+</sup> and M = Mo<sup>6+</sup>, W<sup>6+</sup>) have stimulated much attention over the last few decades.<sup>3</sup> These clusters exhibit strong Brønsted acidity, multi-stage redox activity and remarkable thermal and hydrolytic stability, which are attractive

properties especially in the field of acid and oxidation catalysis. As an example, the 12-phosphotungstic (H<sub>3</sub>PW<sub>12</sub>O<sub>40</sub>, PTA) and 12-phosphomolybdic (H<sub>3</sub>PMo<sub>12</sub>O<sub>40</sub>, PMA) Keggin acids have been used to a great extent in various industrially important catalytic processes, including oxidative hydration and esterification of olefins and catalytic oxidation of alcohols and alkenes.<sup>2,4</sup>

However, the bulk POMs have low surface area (<10 m<sup>2</sup> g<sup>-1</sup>) and exhibit difficulties in separation from reaction media, which significantly restrict their application in many catalytic reactions. To overcome these limitations and, therefore, to improve the catalytic performance, the POM clusters are dispersed on high-surface-area nanoporous supports.<sup>5</sup> Obvious advantages of supported POMs over primary POM clusters are the easier separation from reaction mixtures and recycling without losing their catalytic activity. Supported POMs also offer larger catalytically active surface area compared to the bulk solids and better accessibility of reactants to the active sites. These qualities would favor higher reaction rates and, thus, improvement in catalytic efficiency (*i.e.* catalytic conversion/ moles of catalyst/ reaction time).

Nanoporous POM-based materials are usually prepared by wet impregnation of soluble POM clusters onto the surface of inorganic supports such as porous silica,<sup>6</sup> alumina,<sup>7</sup> titania<sup>7</sup> and zirconia.<sup>8</sup> Although this is a simple method which may yield mesoporous solids with improved catalytic performance, the impregnating synthesis suffers from several drawbacks such as difficulties in homogeneous dispersion of POM units and pores blocking of inorganic support. Also, it has been demonstrated that the impregnated POM clusters are susceptible to leaching in polar solvents when deposited on weak acid or neutral supports (*e.g.* SiO<sub>2</sub>)<sup>9</sup> or structure decomposition when deposited on

<sup>a</sup>Department of Materials Science and Technology, University of Crete, Heraklion, 71003, Crete, Greece. E-mail: garmatas@materials.uoc.gr; Fax: +30-2810-545197; Tel: +30-2810-545004

<sup>b</sup>Department of Chemistry, University of Ioannina, Ioannina, 45110, Greece

supports with strong basic character (*e.g.*  $\text{Al}_2\text{O}_3$ ,  $\text{MgO}$ ).<sup>10</sup> The inclusion of POMs in a mesoporous framework is a promising synthetic approach for stable and highly active catalysts.<sup>11</sup> So far, the synthesis of mesoporous POM-based composites is mostly based on surfactant-assisted sol-gel copolymerization of silicon hydroxides ( $\text{Si}(\text{OH})_4$ ) and POM anions. These materials feature a silica-based heteropoly acid framework with large internal surface area ( $>200 \text{ m}^2 \text{ g}^{-1}$ ) and regular mesoporosity.<sup>9</sup> However, the POM clusters interact weakly with the silanol groups and, therefore, they can be easily leached out from the walls when a polar solvent or reactant is used.<sup>12</sup> This decreases tremendously the applicability of these materials especially in heterogeneous catalysis.

Zirconia ( $\text{ZrO}_2$ ) has received considerable attention because of its semiconducting properties, high thermal stability, reducing character and acid-base bifunctional activity.<sup>13</sup> Owing to these features, zirconia-based materials are potentially applicable in redox and photo-catalysis. Recent studies have indicated that mesoporous zirconia is suitable for supporting POM anions *via* relatively strong chemical bonds.<sup>14</sup> Indeed, the POM clusters immobilized on  $\text{ZrO}_2$  can exhibit strong acid and redox character.<sup>15</sup> To the best of our knowledge, no systematic synthesis of zirconia-based POM composite frameworks with tunable composition and ordered mesostructure has been reported.

Generally, the synthesis of mesoporous POM-based composites by sol-gel inclusion is a complicated and difficult procedure. The low processability of POM clusters to create ordered mesostructures and the difficulty in removing the surfactant inside the pores are the main limitations towards open-pore POM-based mesostructures. Furthermore, the POM anions can perturb the long-range order of organic and inorganic aggregates due to their tendency to interact strongly with the surfactant micelles.<sup>16</sup>

Herein, we report the first example of periodically ordered mesoporous frameworks consisting of nanocrystalline  $\text{ZrO}_2$  and Keggin 12-phosphomolybdic acid compounds through a surfactant-templating method. Pure mesoporous zirconia was also prepared without addition of heteropoly acids. These materials possess a well-ordered pore structure in hexagonal  $p6mm$  symmetry with uniform mesopores. The mesoporous  $\text{ZrO}_2$ -PMA composites demonstrated great application potential in "green" organic synthesis, exhibiting exceptional stability and catalytic activity in oxidation of alkenes using hydrogen peroxide as oxidant.

## 2. Experimental

### 2.1 Chemical reagents

12-Phosphomolybdic acid (PMA) was purchased from Alfa Aesar. This solid was heated at  $100 \text{ }^\circ\text{C}$  for 4 h in air to eliminate the excess of uncoordinated water molecules. When the 12-phosphomolybdic acid was thermally treated, the color changes from yellow to green, which can be interpreted by the formation of Mo(V) species (*i.e.* formation of mixed-valence  $\text{H}_{n>3}\text{PMo}_{12}\text{O}_{40}$  compounds).<sup>17</sup> The weight proportion of water ( $\sim 4.6\%$ ) on the dried sample was determined by thermogravimetric analysis (TGA), obtaining a molecular formula of  $\text{H}_3\text{PMo}_{12}\text{O}_{40}\cdot 5\text{H}_2\text{O}$  (assuming that the protonation state of the polyanions has

a negligible effect on the formula weight). The alkenes used as substrates were of high purity and commercially available from Sigma-Aldrich.

### 2.2 Preparation of mesoporous $\text{ZrO}_2$ -PMA nanocomposites

In a typical preparation of mesoporous zirconia and  $\text{ZrO}_2$ -PMA composites, 0.5 g of triblock copolymer Pluronic F127 ( $\text{EO}_{106}\text{PO}_{70}\text{EO}_{106}$ ,  $M_{\text{av}} = 12600$ , Sigma-Aldrich) was dissolved in 10 ml of anhydrous ethanol ( $>99.5\%$ ), forming a clear solution. Then, 1.6 g (5 mmol) of zirconium oxide dichloride ( $\text{ZrOCl}_2\cdot 8\text{H}_2\text{O}$ , Sigma-Aldrich) was added to the surfactant solution and the mixture was stirred vigorously for  $\sim 2$  h at room temperature. After this, a clear solution of PMA in 1 ml ethanol was added dropwise and the resulting mixture was allowed to continue stirring at room temperature for another  $\sim 10$  min. The homogeneous sol underwent solvent evaporation at  $40 \text{ }^\circ\text{C}$  for 3 days and the foam-like product was dried at  $100 \text{ }^\circ\text{C}$  under vacuum for 12 h. The template was removed by calcination at  $250 \text{ }^\circ\text{C}$  with a heating rate of  $0.5 \text{ }^\circ\text{C min}^{-1}$  and held for 4 h and, then, at  $350 \text{ }^\circ\text{C}$  with a heating rate of  $0.5 \text{ }^\circ\text{C min}^{-1}$  and held for 6 h in air. A series of mesoporous  $\text{ZrO}_2$ -PMA composites, designated as ZPMA(*w*), with PMA loadings (*w*) of 12, 22 and 37 wt% was prepared by using 0.05, 0.1 and 0.2 mmol of 12-phosphomolybdic acid, respectively. Mesoporous zirconia (meso- $\text{ZrO}_2$ ) was also prepared following a procedure similar to that described above, without the presence of 12-phosphomolybdic acid. For comparative studies, the impregnated PMA sample, designated by PMA(37)/ $\text{ZrO}_2$ , was also prepared by suspending 0.1 g of mesoporous zirconia (dried at  $150 \text{ }^\circ\text{C}$ ) in 5 ml of ethanol containing 30 mg of PMA. The slurry was vigorously stirred for 1 h and the solvent was evaporated slowly at  $60 \text{ }^\circ\text{C}$ . The solid product was dried at  $100 \text{ }^\circ\text{C}$  overnight and then calcined at  $350 \text{ }^\circ\text{C}$  for 6 h in air. The PMA content of the impregnated PMA(37)/ $\text{ZrO}_2$  sample was close to that of the ZPMA(37) composite.

### 2.3 Physical characterization

Small-angle X-ray scattering (SAXS) patterns were recorded on a Rigaku S-MAX 3000 high-brilliance system equipped with a two-dimensional wire detector and a Cu ( $\lambda = 1.54098 \text{ \AA}$ ) rotating anode operated at 80 kV and 40 mA ( $0.01 < q < 0.6 \text{ \AA}^{-1}$ ). Measurements were performed by transmission in samples that were gently ground and held in a quartz capillary tube (I.D. 1 mm). The sample to detector distance and the center of the beam were precisely determined by calibration with Ag-behenate diffraction standard ( $d_{001} = 58.38 \text{ \AA}$ ). The diffraction intensities of two-dimensional collected images were integrated to yield one-dimensional diffraction patterns as a function of *q* vector with the FIT2D program.<sup>18</sup> Scattering data were corrected for dark current and empty tube scattering. Nitrogen adsorption-desorption isotherms were measured at 77 K on a Micromeritics TriStar II 3020 sorption analyzer. Before the measurements the samples were outgassed at  $150 \text{ }^\circ\text{C}$  under vacuum ( $<10^{-5}$  Torr) for 15 h. The surface areas were calculated using the Brunauer-Emmett-Teller (BET) method<sup>19</sup> on the adsorption data in the relative pressure range of 0.05–0.2. The total pore volumes were derived from the adsorbed amount at the relative pressure of  $P/P_0 = 0.95$  and the pore size distributions were calculated from

the adsorption branch of the isotherms using the NLDFT method.<sup>20</sup> Transmission electron microscopy (TEM) was carried out on a JEOL JEM-2100 electron microscope equipped with a LaB<sub>6</sub> filament and operating at 200 kV. The samples were first gently ground, suspended in ethanol by sonication and then picked up on a Cu grid covered with a carbon film. Quantitative microprobe analyses were performed on a JEOL JSM-6390LV scanning electron microscope (SEM) equipped with an INCA PentaFETx3 (Oxford Instruments) energy dispersive X-ray (EDX) spectroscopy detector. Data acquisition was performed with an accelerating voltage of 20 kV and 60 s accumulation time. The wide-angle XRD data were recorded on an Inel X-ray diffractometer (40 kV, 20 mA) equipped with Ni-filtered Cu K $\alpha$  radiation ( $\lambda = 1.5405 \text{ \AA}$ ) in Debye–Scherrer geometry. Infrared spectra of solid samples were obtained on a Thermo Nicolet 6700 FT-IR spectrometer. Spectra were obtained on fine powders in diffused reflectance (DRIFT) mode under nitrogen atmosphere and averaging 254 interferograms with a resolution of  $2 \text{ cm}^{-1}$ . UV/vis/NIR diffuse reflectance spectra were recorded at room temperature on a Shimadzu UV-3101PC double-beam, double monochromator spectrophotometer, using powder BaSO<sub>4</sub> as a 100% reflectance standard. Reflectance data were converted to absorption ( $\alpha/S$ ) according to the Kubelka–Munk equation:  $\alpha/S = (1 - R)^2/(2R)$ , where  $R$  is the reflectance, and  $\alpha$  and  $S$  are the absorption and scattering coefficients, respectively.

## 2.4 Catalytic reactions

Catalytic reactions were carried out in 5 ml glass vials equipped with stirring bars. The reaction was initiated by slowly adding (within a period of 5 min) the oxidant H<sub>2</sub>O<sub>2</sub> into a CH<sub>3</sub>CN solution containing the catalyst and the substrate at 50 °C. As an internal standard, acetophenone or bromobenzene was used. The products of the reaction were identified and quantified on a Shimadzu GC-17A gas chromatograph coupled with a GCMS-QP5000 mass spectrometer, by withdrawing small aliquots from the reaction mixture. The yields reported herein are based on the amount of oxidant H<sub>2</sub>O<sub>2</sub> introduced. To establish the identity of the products unequivocally, the retention times and spectral data were compared to those of commercially available compounds. Blank experiments showed that without catalyst the oxidative reactions do not take place.

## 3. Results and discussion

### 3.1 Synthesis and structural characterization

The synthesis of mesoporous ZrO<sub>2</sub>-based phosphomolybdic acid materials was accomplished by controlled cross-linking polymerization of zirconium oxide dichloride (ZrOCl<sub>2</sub>) and PMA compounds in the presence of nonionic triblock (ethylene oxide)<sub>106</sub>-*b*-(propylene oxide)<sub>70</sub>-*b*-(ethylene oxide)<sub>106</sub> copolymer surfactant. The synthetic procedure involves evaporation-induced cooperative assembly of inorganic species and surfactants in ethanolic solution. In this process, the Zr–OH groups of zirconium oxides maybe protonated in the acid medium of PMA giving  $(\equiv\text{Zr}-\text{OH}_2^+)_x\{\text{H}_{n-x}\text{PMO}_{12}\text{O}_{40}\}$  compounds by an acid–base reaction. Such ionic compounds can interact *via* electrostatic and hydrogen bonding interactions with the hydrophilic poly(ethylene oxide) segments of the surfactant forming

mesostructured arrays of inorganic–organic components. By varying the amount of PMA used in the sol–gel process, a series of ordered mesoporous ZPMA(*w*) materials having different loadings ( $w = 12, 22$  and  $37 \text{ wt\%}$ ) of PMA clusters was obtained. Note that the ZrOCl<sub>2</sub> precursor was found to be suitable for the construction of well-organized mesostructures. Attempts to prepare mesoporous ZrO<sub>2</sub>–PMA composites using other zirconium compounds, like zirconium *n*-alkoxide (Zr(OBu)<sub>4</sub>) and zirconium chloride (ZrCl<sub>4</sub>), resulted in somewhat disordered mesostructures. Also, addition of HCl as an inhibitor agent to the zirconium oxo-hydroxides condensation does not improve the long-range order, and gives mesoporous with wormhole-like pore structure.

The mesoscopic order of the title materials was confirmed with small-angle X-ray scattering (SAXS) and transmission electron microscopy (TEM). The SAXS patterns of template-free mesoporous zirconia (meso-ZrO<sub>2</sub>) and ZPMA(*w*) composites showed an intense diffraction peak at a  $q$  scattering vector ( $=4\pi \sin \theta/\lambda$ , where  $2\theta$  is the scattering angle) range of  $0.70\text{--}0.80 \text{ nm}^{-1}$  and two weak but well-resolved diffraction peaks around  $1.13\text{--}1.56 \text{ nm}^{-1}$  range with a  $q$ -value ratio of  $1 : \sqrt{3} : \sqrt{4}$  (Fig. 1a). These peaks can be indexed as the 100, 110 and 200 Bragg reflections of the 2D hexagonal  $p6mm$  structure. The broadening of the main diffraction peaks of ZPMA(*w*) relative to the mesoporous zirconia implies a decrease in the coherent domain size in composite mesostructures. The position of 100 diffractions is associated with an interplanar distance ( $d = 2\pi/q$ ) from 7.89 to 9 nm, which gives a hexagonal lattice parameter ( $a_0$ ) from  $\sim 9.1$  to  $\sim 10.4 \text{ nm}$ . In Fig. 1b, the wide-angle X-ray diffraction (XRD) patterns of mesoporous samples showed several weak diffraction peaks in the  $2\theta$  range of  $30\text{--}75^\circ$ , which can be indexed as the 011, 110, 012, 112, 121, 202 and 220 Bragg reflections of tetragonal ZrO<sub>2</sub> phase (PDF no. 50-1089). The weakness of these peaks makes it difficult to determine the crystallite size, however, their broadness obviously indicates the nanocrystalline property of these materials. Generally, the tetragonal phase of ZrO<sub>2</sub> is thermodynamically unstable at room temperature and it can be stabilized in ZrO<sub>2</sub> nanocrystallites of coherent size below 30 nm.<sup>21</sup> The absence of diffraction peaks associated with the

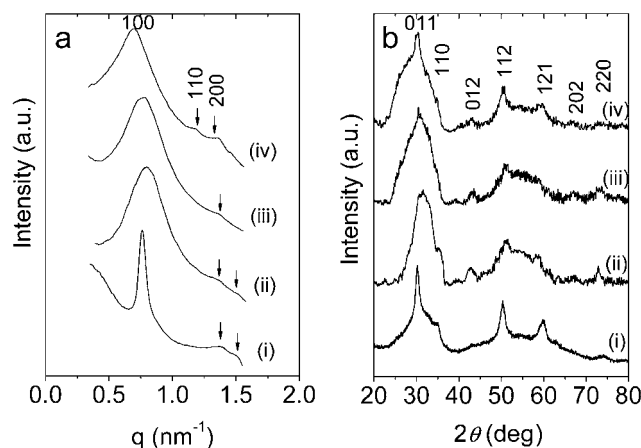


**Fig. 1** (a) SAXS and (b) wide-angle XRD patterns of mesoporous materials: (i) meso-ZrO<sub>2</sub>, (ii) ZPMA(12), (iii) ZPMA(22) and (iv) ZPMA(37).

crystalline phase of PMA in wide-angle XRD patterns implies rather a high dispersion of these clusters into the frameworks.

Fig. 2a–d display typical TEM images and the corresponding fast-Fourier transform (FFT) patterns obtained from mesoporous ZPMA(12) and ZPMA(37) samples. The TEM images clearly show a long-range hexagonal arrangement of parallel pore channels along the [001] and [110] directions, providing further evidence for the well-ordered 2D hexagonal  $p6mm$  mesostructure. TEM analysis indicates an average pore-to-pore distance of  $\sim 9.2$  and  $\sim 10.3$  nm and pore diameter of  $\sim 5$  nm for mesoporous ZPMA(12) and ZPMA(37), respectively. This gives an estimation for the pore wall thickness at  $\sim 4.2$  nm for ZPMA(12) and  $\sim 5.3$  nm for ZPMA(37), in very good agreement with the results from SAXS and  $N_2$  porosimetry (see below). A multicrystalline feature of the pore wall structure of ZPMA(12) was also evidenced with select-area electron diffraction (SAED), Fig. 2e. The SAED pattern shows a series of spotted Debye–

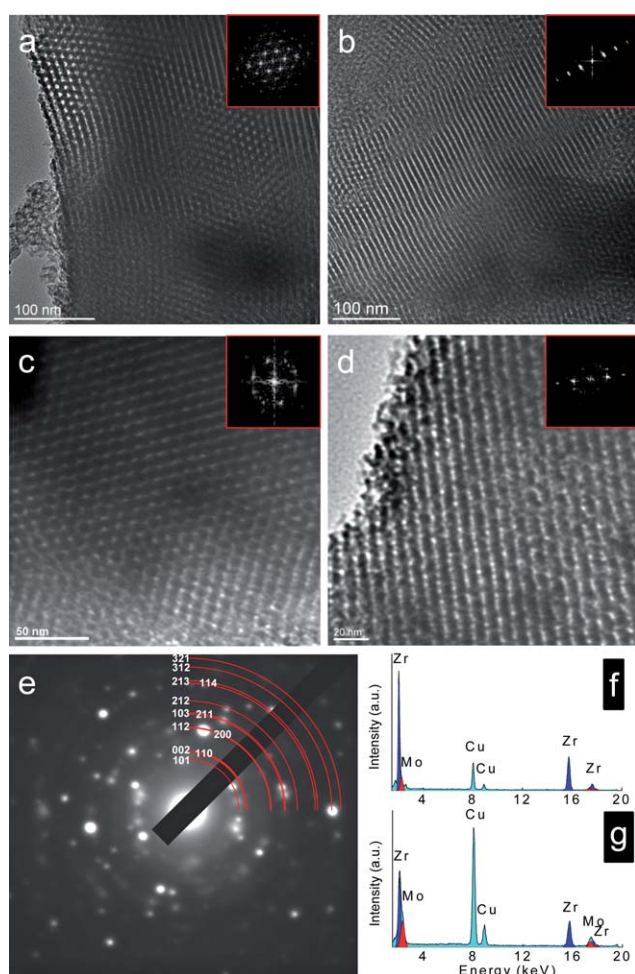


**Fig. 2** Typical TEM images and the corresponding fast Fourier transform patterns (insets) of the mesoporous (a and b) ZPMA(12) and (c and d) ZPMA(37) taken along the [001] (a and c) and [110] (b and d) zone axes, showing the hexagonal array of uniform pore channels. (e) SAED pattern taken along a thin area of mesoporous ZPMA(12). The red lines show the Debye–Scherrer rings of tetragonal  $ZrO_2$  phase ( $a = 3.6008$  Å and  $c = 5.1793$  Å; space group:  $P42/nmc$ ). EDX spectra obtained on TEM for mesoporous ZPMA(12) (f) and ZPMA(37) (g) samples. The copper peaks result from the TEM grid.

Scherrer diffraction rings, which are reasonably assigned to the tetragonal  $P42/nmc$  crystal structure of  $ZrO_2$ .

To ascertain the presence of phosphomolybdic acids within the inorganic frameworks, we also determined the elemental composition of the local structure of ZPMA(12) and ZPMA(37) samples by TEM energy dispersive X-ray (EDX) analysis. The TEM-EDX spectra acquired across a thin area of the mesoporous structures indicate a Zr/Mo atomic ratio of  $\sim 8.90$  and  $\sim 2.14$  for mesoporous ZPMA(12) and ZPMA(37), respectively (Fig. 2f and g). These ratios correspond to a weight percentage of PMA loading at  $\sim 12.2$  for ZPMA(12) and  $\sim 36.5$  for ZPMA(37), which are consistent very well with the nominal compositions. This suggests that the PMA clusters are mainly located within the frameworks and not aggregated as a separated phase.

The mesoporosity of template-free zirconia and ZPMA( $w$ ) materials was probed with nitrogen physisorption measurements. All samples reveal  $N_2$  adsorption–desorption isotherms of type-IV according to the IUPAC classification, with a distinct condensation step at a relative pressure ( $P/P_0$ ) range of  $\sim 0.4$  to  $0.5$ , suggesting narrow sized mesopores (Fig. 3). The small hysteresis loop between the adsorption and desorption branches resembles those of  $H_1$  and  $H_2$ -type and it is consistent with the presence of intermediate pore channels between cylindrical and

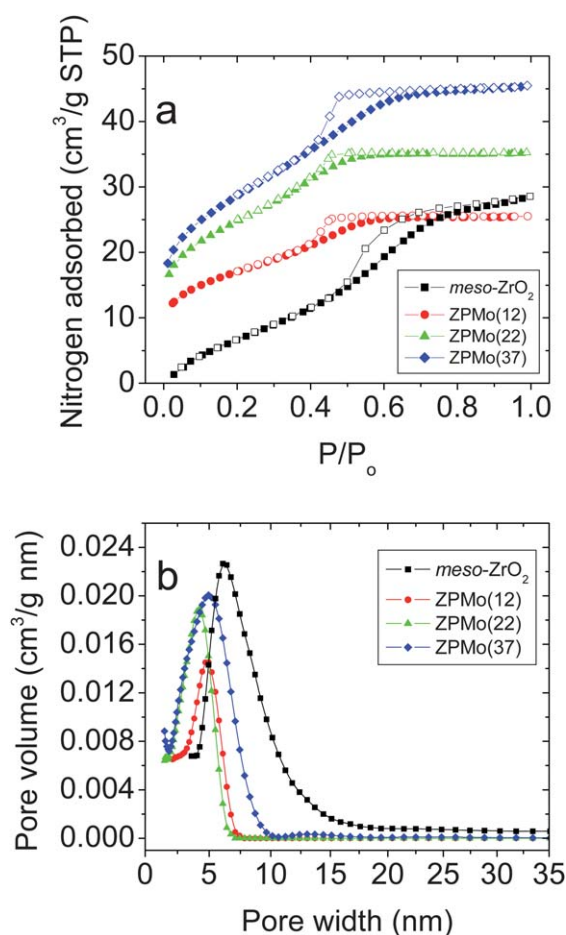


**Fig. 3** (a) Nitrogen adsorption–desorption isotherms at 77 K of mesoporous zirconia ( $meso-ZrO_2$ ) and ZPMA( $w$ ) composites. For clarity, the isotherms of  $meso-ZrO_2$  are offset along the  $y$  axis by  $-5$   $cm^3 g^{-1}$ . (b) NLDFT pore size distributions calculated from adsorption branches.

cage-like shapes.<sup>22</sup> It is plausible some of the PMA clusters to be located near the surface of mesoporous walls, creating small undulations into the pore channels. The mesoporous zirconia has a Brunauer–Emmett–Teller (BET) surface area of 56 m<sup>2</sup> g<sup>-1</sup> and a pore volume of 0.06 cm<sup>3</sup> g<sup>-1</sup>, while mesoporous ZPMA(*w*) composites were found to have higher BET surface areas in the range 60–103 m<sup>2</sup> g<sup>-1</sup> and a pore volume in the range 0.04–0.07 cm<sup>3</sup> g<sup>-1</sup> (Table 1). It is noticeable that the surface area of ZPMA(*w*) increases as the loading of PMA clusters increases. This signifies the role of heteropoly acids in self-assembly process, where it is believed that the PMA anions are engaged in specific (van der Waals and/or hydrogen bonding) interactions with the surfactant micelles, promoting the formation of ordered mesostructures with higher porosity. All the textural properties of the mesoporous zirconia and ZPMA(*w*) composites are given in Table 1.

The non-local density function theory (NLDFT) analysis of the adsorption branches of mesoporous zirconia and ZPMA(*w*) composites revealed a quite narrow distribution of the pore sizes, as indicated from the full-width at half maximum (FWHM) of the peaks, with the peak maximum being in the range 4.2–6.2 nm. Despite being templated by the same surfactant, the pore sizes in ZPMA(*w*) composites are smaller than that obtained in mesoporous zirconia, reflecting the strong interactions of the anionic PMo<sub>12</sub>O<sub>40</sub><sup>n-</sup> clusters and (≡Zr–OH<sub>2</sub><sup>+</sup>)<sub>x</sub>{H<sub>n-x</sub>PMo<sub>12</sub>O<sub>40</sub>} species with the surfactant. The NLDFT pore diameters together with the pore-to-pore distance (*a*<sub>0</sub>) from SAXS analysis indicate a framework wall thickness from ~3.3 to ~5.4 nm. It can be observed that the size of pore wall thickness is strongly related to the PMA loading (*w*) and continuously increases as the content of PMA in composite structures is increased (see Table 1). This systematic variation of wall thickness with the PMA loading clearly supports the fact that the phosphomolybdic acids are an integral part of the mesoporous frameworks.

### 3.2 Spectroscopy

The Fourier transform-infrared (FT-IR) spectroscopy is a very sensitive technique to detect the vibrations of metal–oxygen bonds and, thus, can provide important information for the molecular structure of PMA clusters. The FT-IR spectra of pure PMA and mesoporous zirconia and ZPMA(*w*) composites are shown in Fig. 4. The PMA solid exhibited the characteristic absorption bands at ~1066, ~968, ~872 and ~778 cm<sup>-1</sup>, which are attributed to the stretching mode of P–O bonds in the PO<sub>4</sub> tetrahedron, Mo=O terminal bonds, Mo–O<sub>b</sub>–Mo bridge bonds between the corner-sharing MoO<sub>6</sub> octahedra and Mo–O<sub>c</sub>–Mo bridge bonds between the edge-sharing MoO<sub>6</sub> octahedra, respectively.<sup>23</sup> The weak absorption band at ~593 cm<sup>-1</sup> is

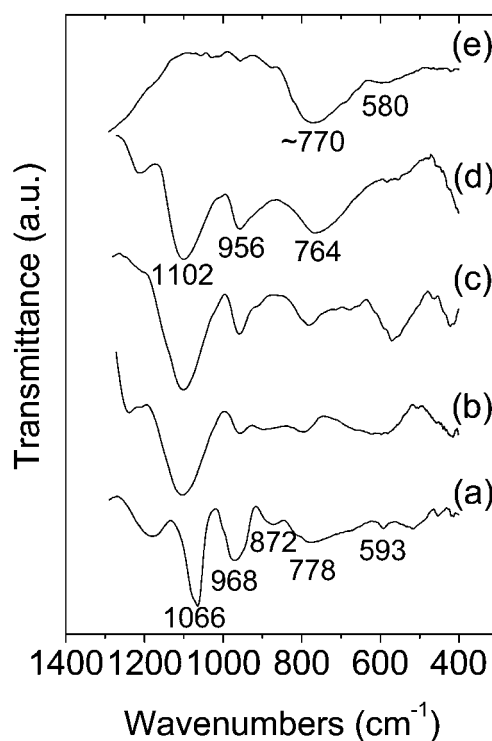


Fig. 4 FT-IR spectra of (a) bulk PMA and mesoporous (b) ZPMA(12), (c) ZPMA(22), (d) ZPMA(37) and (e) meso-ZrO<sub>2</sub> materials.

assigned to the stretching vibration mode of O–P–O bonds.<sup>23b</sup> Compared to the pristine PMA clusters, the ZPMA(*w*) indicated a considerable bathochromic shift (~30 cm<sup>-1</sup>) of the Mo=O and Mo–O<sub>c</sub>–Mo absorption bands at ~956 and ~764 cm<sup>-1</sup> respectively, suggesting strong binding of PMA Keggin units to the zirconia matrix. The intense absorption peak at ~1102 cm<sup>-1</sup> is ascribed to the P–O stretching mode of the distorted PO<sub>4</sub> central unit while the vibrational features at 760–780 cm<sup>-1</sup> and ~580 cm<sup>-1</sup> are assigned to the Zr–O and Zr–O–Zr stretching modes of tetragonal zirconia.<sup>24</sup>

The electronic structure of PMA clusters in the framework of ZPMA(*w*) was probed with ultraviolet-visible-near IR (UV/vis/NIR) spectroscopy. Fig. 5 depicts the diffuse reflectance UV/vis/NIR spectra of pure PMA and mesoporous zirconia and ZPMA(*w*) materials. The PMA exhibits the characteristic absorption peaks at ~46 × 10<sup>3</sup> (217 nm) and ~32 × 10<sup>3</sup> (313 nm) cm<sup>-1</sup> which are attributed to the O(II) → Mo(VI) charge transfer in Mo=O and Mo–O–Mo bonds, respectively.<sup>15</sup> The broad electronic absorption at ~42 × 10<sup>3</sup> cm<sup>-1</sup> (238 nm) possibly corresponds to the electron transition from occupied p-orbitals of O(II) to unoccupied d-orbitals of Mo(V). Further evidence for

Table 1 Textural properties of mesoporous zirconia (meso-ZrO<sub>2</sub>) and ZPMA(*w*) composites

Sample	Surface area/m <sup>2</sup> g <sup>-1</sup>	Pore volume <sup>a</sup> /cm <sup>3</sup> g <sup>-1</sup>	Pore size <sup>b</sup> /nm	<i>d</i> <sub>100</sub> -Spacing/nm	Unit cell <sup>c</sup> /nm	WT <sup>d</sup> /nm
meso-ZrO <sub>2</sub>	56	0.06	6.2 (3.7)	8.235	9.5	3.3
ZPMA(12)	60	0.04	4.9 (3.3)	8.256	9.5	4.6
ZPMA(22)	88	0.05	4.2 (2.9)	7.864	9.1	4.9
ZPMA(37)	103	0.07	5.0 (4.1)	9.001	10.4	5.4

<sup>a</sup> Cumulative pore volume at relative pressure *P/P*<sub>0</sub> = 0.95. <sup>b</sup> In parenthesis: the full-width of the half maximum of pore size distributions. <sup>c</sup> The unit cell parameter is given by *a*<sub>0</sub> = (2/√3)*d*<sub>100</sub>. <sup>d</sup> The framework wall thickness is given by WT = *a*<sub>0</sub> – *D*, where *D* is the pore size.

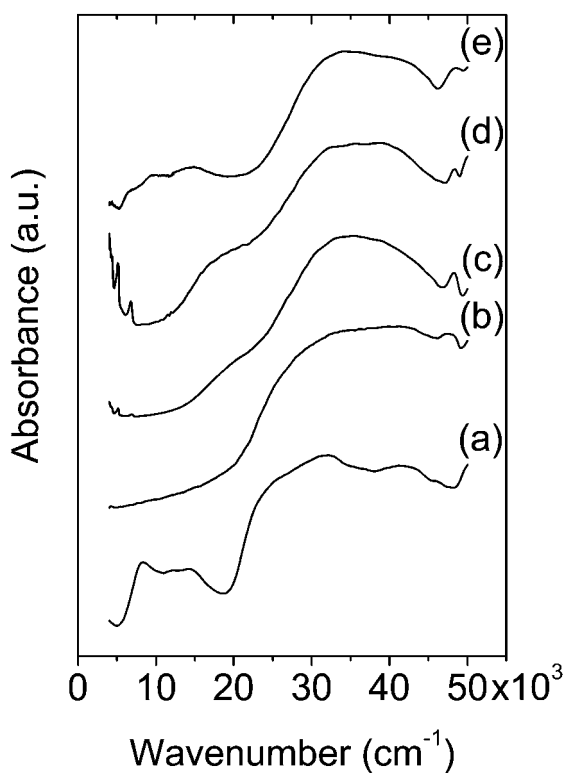
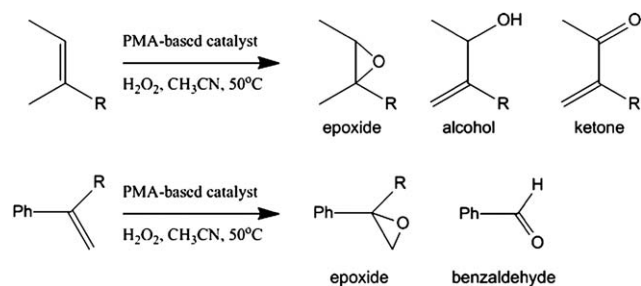


**Fig. 5** Diffuse reflectance UV/vis/NIR spectra of (a) bulk PMA, (b) meso-ZrO<sub>2</sub>, and mesoporous (c) ZPMA(12), (d) ZPMA(22) and (e) ZPMA(37) materials.

the partially reduced form of PMA clusters were obtained by the two absorption bands at  $\sim 14 \times 10^3$  (714 nm) and  $\sim 8.4 \times 10^3$  (1190 nm)  $\text{cm}^{-1}$ , which can be assigned to the d-d transition of the Mo(v) octahedron and the Mo(v)-to-Mo(vi) intervalence transition within the  $\{\text{PMo}_{12}\text{O}_{40}\}^{n-}$  cluster, respectively.<sup>25</sup> Compared to pure PMA, the ZPMA(*w*) composites exhibit a strong hypsochromic shift in oxygen-to-molybdenum absorptions at  $\sim 48 \times 10^3$  (208 nm) and  $\sim 35$  to  $36 \times 10^3$  (270–285 nm)  $\text{cm}^{-1}$  respectively, which may be consistent with the quantum confinement due to the molecular dispersion of PMA within the zirconia network.<sup>26</sup> This is in line with the results from TEM-EDX and wide-angle XRD. Although Mo(v) species in the composite ZPMA(*w*) frameworks are expected due to the incorporated PMA clusters, their presence was clearly evident in the highest loading sample ZPMA(37), judging from the prominent absorptions at  $\sim 15 \times 10^3$  (667 nm) and  $\sim 10 \times 10^3$  (1000 nm)  $\text{cm}^{-1}$ . The weak shoulder at  $\sim 39 \times 10^3$   $\text{cm}^{-1}$  (256 nm) in absorption spectra of ZPMA(*w*) can be attributed to the charge transfer from valence (O 2p) to conduction band (Zr 4d) of ZrO<sub>2</sub>. These absorption bands are significantly bathochromic shifted compared to the mesoporous zirconia ( $\sim 41 \times 10^3$   $\text{cm}^{-1}$ , 244 nm), implying altered electronic structure due to the incorporated PMA clusters.<sup>27</sup>

### 3.3 Catalytic reactivity

The mesoporous ZPMA(*w*) composites were tested in catalytic oxidation of various alkenes using hydrogen peroxide as oxidant (Scheme 1). The hydrogen peroxide is a preferable oxidant for



**Scheme 1** Oxidation reactions of alkenes (R = H-, CH<sub>3</sub>-; Ph = C<sub>6</sub>H<sub>5</sub>-) catalyzed by ZPMA(37).

industrial uses because of its high oxygen donor efficiency, low cost and environmentally friendly considerations.<sup>28</sup> All the oxidation reactions were performed using catalyst/H<sub>2</sub>O<sub>2</sub> (30 wt% in water)/substrate molar ratios of 1 : 50 : 250 in acetonitrile, which proved to be an optimum condition for this system. The optimization was deduced from kinetic profiles of the cyclooctene epoxidation using ZPMA(37) catalyst at 50 °C (Fig. 6). The time courses of cyclooctene oxidation, in Fig. 6, also indicate that higher catalyst-to-substrate molar ratios promote faster reactions at the beginning, which after a period reaches a saturation of conversion. This observation can be explained on the basis of the reactivity of POM clusters with substrates. It has been reported that hydrocarbons in large amounts may be absorbed onto the surface of heteropoly acids that block the active sites, thus decreasing the reaction rate.<sup>29</sup> The decrease of the conversion rate with time can be attributed to the lower concentration of reactants that are available for catalysis during the reaction progress. Next, efforts were directed to investigate the effect of PMA loading of ZPMA(*w*) on hydrogen peroxide mediated catalytic oxidation using cyclooctene as a probe. These results revealed a systematic increase of the catalytic activity as the amount of the incorporated PMA increases (see Table 2). Specifically, the ZPMA(12) and ZPMA(22) showed respectively

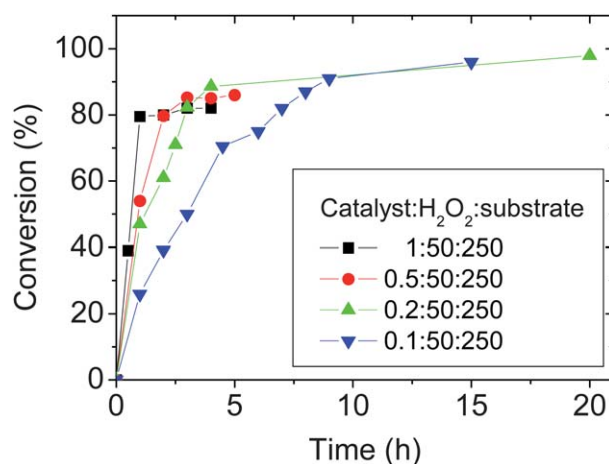


**Fig. 6** Cyclooctene conversion as a function of reaction time in acetonitrile at 50 °C catalyzed by ZPMA(37). The various molar ratios of catalyst/H<sub>2</sub>O<sub>2</sub>/cyclooctene substrate are provided in legend. Conversions are given as mol% of produced cyclooctene epoxide based on the amount of oxidant introduced.

**Table 2** Epoxidation of cyclooctene with H<sub>2</sub>O<sub>2</sub> catalyzed by the series of ZPMA(*w*)<sup>a</sup>

Catalyst	PMA loading <sup>b</sup> (wt%)	Conversion <sup>c</sup> (%)	TOF <sup>d</sup> /h <sup>-1</sup>
meso-ZrO <sub>2</sub>	0	<1	—
ZPMA(12)	12.2	5	3
ZPMA(22)	22.4	22	11
ZPMA(37)	37.2	80	41

<sup>a</sup> Reaction conditions: 2.5 mmol of cyclooctene, 0.01 mmol of catalyst, 0.5 mmol of H<sub>2</sub>O<sub>2</sub> (30 wt% in water), 3 ml CH<sub>3</sub>CN, 50 °C, 1 h. <sup>b</sup> PMA loading based on the nominal compositions. <sup>c</sup> Conversion is given as mol% of initial quantity of oxidant used. <sup>d</sup> Turnover frequency, TOF, is based on moles of cyclooctene converted in time *t* per moles of H<sub>3</sub>PMO<sub>12</sub>O<sub>40</sub>.

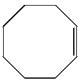
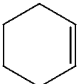
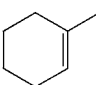
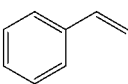
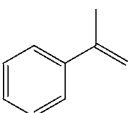
~5% and ~22% yields of cyclooctene epoxide, while the highest loading sample ZPMA(37) reached a maximum catalytic yield of ~80%. Therefore, we used the ZPMA(37) material for all further catalytic studies. As might be expected the mesoporous zirconia does not exhibit any catalytic activity and, therefore, the observed catalytic conversions by ZPMA(*w*) are attributed to the incorporated PMA clusters.

Table 3 summarized the results of the catalytic oxidation of various alkenes catalyzed by heterogeneous ZPMA(37) as well as homogeneous PMA catalyst. It can be observed that the ZPMA(37) achieves 100% selective epoxidation of cyclooctene with high yield (~82%). Indeed, this reaction proceeds very fast (TOF ≈ 41 h<sup>-1</sup>) without the induction period. Oxidation of

cyclohexene and methyl-cyclohexene gave moderate conversions of ~30% and ~26% respectively, forming epoxide and allylic oxidation products. Interestingly, in the case of methyl-cyclohexene, the ZPMA(37) catalyst promotes the epoxidation reaction vs. allylic oxidation with remarkable selectivity (~81%). The oxidation reactions of styrene and methyl-styrene showed a remarkably selective formation of benzaldehyde over epoxide products, however, with moderate yields, implying an oxidative C=C cleavage followed by allylic oxidation. Notably, no diol or acetophenone derivatives were observed as byproducts in these reactions; however, in homogeneous medium, the catalytic oxidations of styrene and methyl-styrene produce additionally considerable amounts of benzylacetaldehyde and benzylmethylketone respectively. The selectivity of ZPMA(37) catalyst to conjugated benzaldehyde was found to be ~95% for styrene and ~61% for methyl-styrene. This suggests an oxidative cleavage of the carbon-carbon double bond of styrene instead of epoxidation, which is less favored in substrates with electron-donating (e.g. methyl) groups substituted on the double bond. Taking into account that methyl-substituted alkenes, as methyl-cyclohexene and methyl-styrene, promote epoxidation reaction vs. allylic oxidation or double bond cleavage, an electrophilic character of the active catalytic unit is suggested.

ZPMA(37) displays comparable or even higher catalytic efficiency than that of other high-performance heterogeneous POM-based catalysts. For example, (X<sup>n+</sup>MW<sub>11</sub>O<sub>39</sub>)<sup>-(10-m)</sup> (where X = P<sup>5+</sup>, Si<sup>4+</sup>; M = Co<sup>2+</sup>, Cu<sup>2+</sup>, Ni<sup>2+</sup>, Mn<sup>2+/3+</sup>) anions immobilized on

**Table 3** Epoxidation of alkenes with H<sub>2</sub>O<sub>2</sub> catalyzed by heterogeneous ZPMA(37) and homogeneous PMA catalysts<sup>a</sup>

Substrate	Conversion <sup>b</sup> (%)	TOF <sup>c</sup> /h <sup>-1</sup>	Selectivity <sup>e</sup> epoxide : alcohol : ketone
Cyclooctene 	82 (99) <sup>c</sup>	41.0 <sup>d</sup> (49.5) <sup>d</sup>	100 : 0 : 0 (100 : 0 : 0)
Cyclohexene 	30 (39)	7.5 (9.7)	47 : 43 : 10 (38 : 44 : 18)
Methyl-cyclohexene 	26 (35)	6.5 (8.5)	81 : 8 : 11 (76 : 12 : 12)
Styrene 	30 (34)	7.5 (8.7)	5 : 0 : 95 <sup>f</sup> (4 : 10 : 86) <sup>f</sup>
Methyl-styrene 	28 (65)	7.0 (16.3)	39 : 61 : 0 <sup>g</sup> (20 : 57 : 23) <sup>g</sup>

<sup>a</sup> Reaction conditions: 2.5 mmol of substrate, 0.01 mmol of catalyst, 0.5 mmol of H<sub>2</sub>O<sub>2</sub> (30 wt% in water), 3 ml CH<sub>3</sub>CN, 50 °C, 2 h. In parenthesis: the catalytic activity and selectivity of homogeneous H<sub>3</sub>PMO<sub>12</sub>O<sub>40</sub> catalyst are given. <sup>b</sup> Total conversion: the amounts of formed products based on the introduced oxidant. <sup>c</sup> Turnover frequency, TOF: moles of products per moles of H<sub>3</sub>PMO<sub>12</sub>O<sub>40</sub> per hour. <sup>d</sup> Reaction time: 1 h. <sup>e</sup> Product selectivity determined based on moles of desired product per moles of all obtained products. <sup>f</sup> Selective formation of epoxide : benzylacetaldehyde : benzaldehyde. <sup>g</sup> Selective formation of epoxide : benzaldehyde : benzylmethylketone.

modified SBA-15 silica showed *ca.* 16–56% conversion of styrene with moderate to high selectivity ( $\sim 76$  to 97%) for benzaldehyde with  $\text{H}_2\text{O}_2$ , but in 12 h.<sup>30</sup> Recently, zirconia catalyst impregnated lacunary ( $\text{PW}_{11}\text{O}_{40}$ )<sup>7-</sup> anions was demonstrated for the oxidation of styrene.<sup>31</sup> This catalyst gives very good activity and selectivity, showing  $\sim 41\%$  styrene conversion with high benzaldehyde selectivity ( $>99\%$ ) after 4 h. Overall, the ZPMA(37) showed remarkable efficacy in oxidation of the examined alkene as indicated from the conversion degrees and the turnover frequencies for all the catalytic reactions (Table 3).

Comparative studies on the oxidation of alkenes using the homogeneous PMA catalyst under the same reaction conditions showed that heterogeneous ZPMA(37) exhibits similar catalytic activity than the pure PMA solid. However, the oxidation reaction by PMA is a homogeneous process since these clusters are very soluble in acetonitrile. These findings support the fact that the zirconia matrix embeds the PMA heteropoly acids without affecting their redox properties and catalytic performance.

The stability of mesoporous ZPMA(37) was examined by repeated recovering–reusing of the catalyst in oxidation reaction of cyclooctene. In each catalytic cycle, the catalyst was recovered by centrifugation, washed with fresh acetonitrile several times and dried at ambient conditions. The ZPMA(37) showed excellent reusability without significant loss of the catalytic activity and selectivity ( $\sim 82\%$  cyclooctene conversion,  $\sim 44 \text{ h}^{-1}$  TOF, 100% selectivity) even after four repeated catalytic cycles (Fig. 7). Scanning electron microscopy (SEM) EDX microanalysis acquired on four times reused sample showed an average Zr/Mo atomic ratio of  $\sim 1.95$  that corresponds to a percentage of PMA loading at  $\sim 38.7 \text{ wt}\%$ . This value is very close to that expected from the stoichiometric composition (*i.e.* 37.2 wt%). Furthermore, the FT-IR spectrum of this sample showed the characteristic Mo=O and Mo–O–Mo vibration bands at  $\sim 957$  and  $\sim 766 \text{ cm}^{-1}$  respectively, reflecting the Keggin structure of the incorporated PMA clusters (Fig. 8). These results clearly support the high durability of the ZPMA(37) catalyst under the specific conditions.

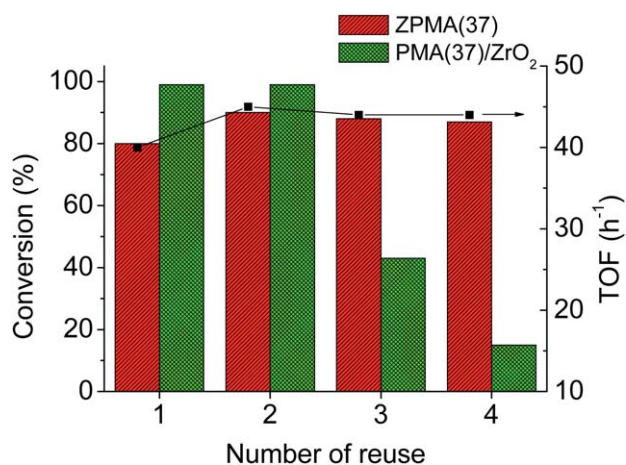


**Fig. 7** Recycle studies of mesoporous ZPMA(37) and impregnated PMA(37)/ZrO<sub>2</sub> catalysts. Reaction conditions: 2.5 mmol of cyclooctene, 0.01 mmol of catalyst, 0.5 mmol of  $\text{H}_2\text{O}_2$  (30 wt% in water), 3 ml  $\text{CH}_3\text{CN}$ , 50 °C, 1 h.

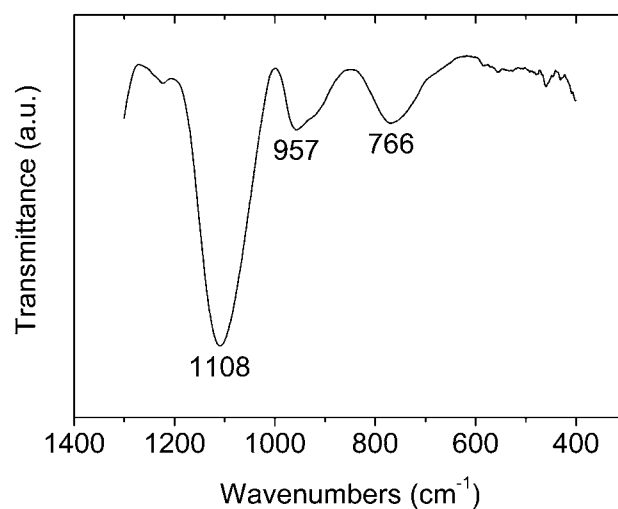


**Fig. 8** Infrared spectrum of four times reused ZPMA(37) catalyst, showing intense peaks at  $\sim 957$  and  $\sim 766 \text{ cm}^{-1}$  that are attributed to the stretching vibration bands of Mo=O and Mo–O–Mo bonds, respectively. The intense peak at  $\sim 1108 \text{ cm}^{-1}$  is assigned to the P–O stretching vibration bands of the distorted  $\text{PMO}_{12}\text{O}_{40}^{3-}$  Keggin structure.

For comparison we also prepared mesoporous PMA(37)/ZrO<sub>2</sub> material by impregnating 37 wt% of 12-phosphomolybdic acid on the surface of mesoporous zirconia (meso-ZrO<sub>2</sub>). This material demonstrates similar PMA content to that of ZPMA(37) and its recyclability was studied under the same reaction conditions. It was found that the impregnated PMA(37)/ZrO<sub>2</sub> catalyst exhibits an excellent yield ( $\sim 99\%$ ) in cyclooctene epoxide in first two catalytic cycles, but its catalytic performance significantly dropped after the third ( $\sim 43\%$ ) and fourth ( $\sim 15\%$ ) catalytic runs (see Fig. 7). These results together with the light green colored filtrates after the separation of solid catalyst witness a significant leaching of PMA during the oxidation reactions. Indeed, the observed catalysis, especially in the first and second run, should be predominantly homogeneous in nature due to the leached PMA clusters. SEM-EDX elemental microanalysis on recovered catalyst indicates a Zr/Mo atomic ratio of  $\sim 8.58$  that corresponds to a weight percentage of PMA loading at  $\sim 12.6 \text{ wt}\%$ . This suggests a considerable loss of PMA clusters ( $\sim 66\%$ ) from the PMA(37)/ZrO<sub>2</sub> solid under the present conditions.

#### 4. Conclusion

A series of mesoporous composite frameworks containing zirconium oxide and 12-phosphomolybdic acid compounds was prepared by using the evaporation-induced cooperative assembly method. The synthetic procedure involved controlled cross-linking copolymerization of zirconium oxo-hydroxide species and PMA anions in the presence of nonionic block copolymer surfactants. The obtained materials possess a well-ordered hexagonal mesostructure with large pore widths (*ca.* 4–6 nm). The pore walls constituted by nanocrystalline ZrO<sub>2</sub> and Keggin PMA clusters with different PMA loadings (*i.e.* 12, 22 and 37 wt%). FT-IR and UV/vis/NIR spectroscopy demonstrated that the Keggin structure of PMA clusters is preserved intact into the mesoporous frameworks, forming a solid solution with the ZrO<sub>2</sub> species. Catalytic studies showed that the resulting mesoporous



ZrO<sub>2</sub>–PMA materials are active in the oxidation reaction of various industrially important alkenes using hydrogen peroxide as oxygen donor. The ZrO<sub>2</sub> loaded with ~37 wt% of PMA demonstrates remarkable catalytic activities which are comparable to those of free PMA clusters, while exhibiting exceptional durability and reusability in oxidation reactions, more than analogously impregnated catalysts. These results indicate that such materials should have great application potential in oxidation catalysis. Because of the well-ordered pore structure, size- and shape-selective catalysis may also be envisioned.

## Acknowledgements

This research was supported by the European Community under Marie Curie International Reintegration Grant (MCIRG No. 230868) and the University of Crete—Special Account for Research (KA 2863). We gratefully thank Prof. M. G. Kanatzidis (Northwestern University) for the use of SAXS and N<sub>2</sub> porosimetry equipment.

## Notes and references

- 1 A. Müller, F. Peters, M. T. Pope and D. Gatteschi, *Chem. Rev.*, 1998, **98**, 239.
- 2 I. V. Kozhevnikov, *Catalysis for Fine Chemical Synthesis: Catalysis by Polyoxometalates*, Wiley-VCH, England, 2002, vol. 2.
- 3 T. Yamase, M. Pope, *Polyoxometalate Chemistry for Nano-Composite Design*, Kluwer Academic Publishers, New York, 2002.
- 4 (a) M. V. Vasylyev and R. Neumann, *J. Am. Chem. Soc.*, 2004, **126**, 884; (b) Y. Nishiyama, Y. Nakaqawa and N. Mizuno, *Angew. Chem., Int. Ed.*, 2001, **40**, 3639; (c) R. Neumann and M. Gara, *J. Am. Chem. Soc.*, 1995, **117**, 5066; (d) C. F. Oliveira, L. M. Dezaneti, F. A. C. Garcia, J. L. de Macedo, J. A. Dias, S. C. L. Dias and K. S. P. Alvim, *Appl. Catal., A*, 2010, **372**, 153.
- 5 (a) S. Uchida, M. Hashimoto and N. Mizuno, *Angew. Chem., Int. Ed.*, 2002, **41**, 2814; (b) K. Zhu, J. Hu, X. She, J. Liu, Z. Nie, Y. Wang, C. H. F. Peden and J. H. Kwak, *J. Am. Chem. Soc.*, 2009, **131**, 9715; (c) K. Inumaru, T. Ishihara, Y. Kamiya, T. Okuhara and S. Yamanaka, *Angew. Chem., Int. Ed.*, 2007, **46**, 7625.
- 6 A. Lapkin, B. Bozkaya, T. Mays, L. Borello, K. Edler and B. Crittenden, *Catal. Today*, 2003, **81**, 611.
- 7 L. R. Pizzio, C. V. Caceres and M. N. Blanco, *Appl. Catal., A*, 1998, **167**, 283.
- 8 X. Qu, Y. Guo and C. Hu, *J. Mol. Catal. A: Chem.*, 2007, **262**, 128.
- 9 P. Vazquez, L. Pizzio, G. Romanelli, J. Autino, C. Caceres and M. Blanco, *Appl. Catal., A*, 2002, **235**, 233.
- 10 (a) S. Hodjati, K. Vaezzadeh, C. Petit, V. Pitchon and A. Kiennemann, *Top. Catal.*, 2001, **16–17**, 151; (b) L. R. Pizzio, P. G. Vazquez, C. V. Caceres and M. N. Blanco, *Appl. Catal., A*, 2003, **256**, 125.
- 11 Y. Guo, K. Li and J. H. Clark, *Green Chem.*, 2007, **9**, 839.
- 12 (a) J. Haber, K. Pamin, L. Matachowski and D. Mucha, *Appl. Catal., A*, 2003, **256**, 141; (b) F. Marme, G. Coudurier and G. Vedrine, *Microporous Mesoporous Mater.*, 1998, **22**, 151; (c) P. Vazquez, L. Pizzio, G. Romanelli, J. Autino, C. Caceres and M. Blanco, *Appl. Catal., A*, 2002, **235**, 233.
- 13 (a) T. Yamaguchi, *Catal. Today*, 1994, **20**, 199; (b) J. Kaspar, P. Fornasiero and N. Hickey, *Catal. Today*, 2003, **77**, 419.
- 14 (a) C. Trolliet, G. Coudurier and J. C. Vedrine, *Top. Catal.*, 2001, **15**, 73; (b) L. Pizzio, P. Vazquez and M. N. Blanco, *Catal. Lett.*, 2001, **77**, 233; (c) P. Sharma and A. Patel, *Appl. Surf. Sci.*, 2009, **255**, 7635.
- 15 E. Lopez-Salinas, J. G. Hernandez-Cortez, M. Cortez, J. Navarrete, M. Yanos, A. Vazquez, H. Armendaris and T. Lopez, *Appl. Catal.*, 1998, **175**, 43.
- 16 (a) R. Neumann and I. Assael, *J. Chem. Soc., Chem. Commun.*, 1989, 547; (b) X. Lin, Y. Wang and L. Wu, *Langmuir*, 2009, **25**, 6081.
- 17 (a) R. Fricke and G. Öhlmann, *J. Chem. Soc., Faraday Trans. 1*, 1986, **82**, 263; (b) E. Blouet-Crussion, M. Rigole, M. Fournier, A. Aboukaïs, F. Daubrege, G. Hecquet and M. Guelton, *Appl. Catal., A*, 1999, **178**, 69.
- 18 F. A. P. Hammersley, *ESRF98HA01T: FIT2D V9.129 reference Manual V3.1, Internal Report*, ESRF, France, 1998.
- 19 S. Brunauer, L. S. Deming, W. S. Deming and E. Teller, *J. Am. Chem. Soc.*, 1940, **62**, 1723.
- 20 P. I. Ravikovitch, D. Wei, W. T. Chueh, G. L. Haller and A. V. Neimark, *J. Phys. Chem. B*, 1997, **101**, 3671.
- 21 (a) R. C. Garvie, *J. Phys. Chem.*, 1978, **82**, 218; (b) S. Shukla and S. Seal, *J. Phys. Chem. B*, 2004, **108**, 3395.
- 22 F. Kleitz, L. A. Solvyov, G. M. Anilkumar, S. H. Choi and R. Ryoo, *Chem. Commun.*, 2004, 1536.
- 23 (a) C. Rocchicciolo-Deltcheff, M. Gournier, R. Franck and R. Thouvenot, *Inorg. Chem.*, 1983, **22**, 207; (b) N. Essayem, A. Holmqvist, P. Y. Gayraud, J. C. Vedrine and Y. Ben Taarit, *J. Catal.*, 2001, **197**, 273.
- 24 (a) K. Nakamoto, *Infrared and Raman Spectra of Inorganic and Coordination Compounds*, 4th edn, Wiley-VCH, New York, 1986; (b) E. Lopez-Salinas, J. G. Hernandez-Cortez, I. Schifter, E. Torres-Garc and T. Lopez, *Appl. Catal., A*, 2000, **193**, 215.
- 25 C. Sanchez, J. Livage, J. P. Launay, M. Fournier and Y. Jeannin, *J. Am. Chem. Soc.*, 1982, **104**, 3194.
- 26 X. K. Yang, L. F. Chen, J. A. Wang, L. E. Norena and O. Novaro, *Catal. Today*, 2009, **148**, 160.
- 27 X. Qu, Y. Guo and C. Hu, *J. Mol. Catal. A: Gen.*, 2007, **262**, 128.
- 28 G. Strukul, *Catalytic Oxidations with Hydrogen Peroxide as Oxidant*, Kluwer Academic, Netherlands, 1992.
- 29 (a) M. Misono, N. Mizuno, K. Katamura, A. Kasai, Y. Konishi, K. Sakata, T. Okuhara and Y. Yoneda, *Bull. Chem. Soc. Jpn.*, 1982, **55**, 400; (b) K. Takahashi, T. Okuhara and M. Misono, *Chem. Lett.*, 1985, 841.
- 30 J. Hu, K. Li, W. Li, F. Ma and Y. Guo, *Appl. Catal., A*, 2009, **364**, 211.
- 31 P. A. Shringarpure and A. Patel, *Dalton Trans.*, 2010, **39**, 2615.